PAPER

Fundamental understanding of millipede morphology and locomotion dynamics

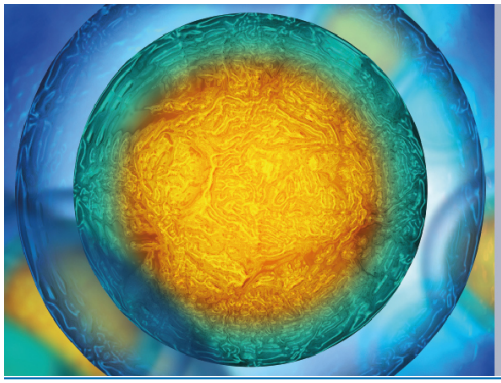

Bioinspiration & Biomimetics

PAPER

Fundamental understanding of millipede morphology and locomotion dynamics

RECEIVED
15 June 2020

REVISED
15 September 2020

ACCEPTED FOR PUBLICATION
2 October 2020

PUBLISHED
21 December 2020

Anthony Garcia[1,2,*], **Gregory Krummel**[1] **and Shashank Priya**[1,3]

[1] Center for Energy Harvesting Materials and Systems (CEHMS), Bio-Inspired Materials and Devices Laboratory (BMDL), Virginia Tech, Blacksburg, VA 24061, United States of America
[2] University of Mary, Bismarck ND 58504, United States of America
[3] Department of Material Science and Engineering, Pennsylvania State University Park, PA 16802, United States of America
[*] Author to whom any correspondence should be addressed.

E-mail: ajgarcia@umary.edu

Keywords: millipede, locomotion, bio-inspired robotics, dynamics, wave

Supplementary material for this article is available online

Abstract

A detailed model for the locomotory mechanics used by millipedes is provided here through systematic experimentation on the animal and validation of observations through a biomimetic robotic platform. Millipedes possess a powerful gait that is necessary for generating large thrust force required for proficient burrowing. Millipedes implement a metachronal gait through movement of many legs that generates a traveling wave. This traveling wave is modulated by the animal to control the magnitude of thrust force in the direction of motion for burrowing, climbing, or walking. The quasi-static model presented for the millipede locomotion mechanism matches experimental observations on live millipedes and results obtained from a biomimetic robotic platform. The model addresses questions related to the unique morphology of millipedes with respect to their locomotory performance. A complete understanding of the physiology of millipedes and mechanisms that provide modulation of the traveling wave locomotion using a metachronal gait to increase their forward thrust is provided. Further, morphological features needed to optimize various locomotory and burrowing functions are discussed. Combined, these results open opportunity for development of biologically inspired locomotory methods for miniaturized robotic platforms traversing terrains and substrates that present large resistances.

1. Introduction

Research in understanding and implementing bio-inspired locomotion has enabled effective locomotion methods for robotic platforms encountering various terrains. The morphology and locomotion of next-generation robots have been influenced by the locomotory capabilities of small insects and other animals that live in the natural environments whose anatomy is adapted for efficiency at various desired scales [1–7]. Prior research has garnered inspiration from the locomotion of arthropods such as six-legged insects and eight-legged arachnids with rigid-bodies. Such morphologies have stability, flexibility and adaptability limitations, particularly in miniature robotic applications where locomotion is constrained. This can be illustrated in an example where damage to a single leg in a six-legged platform can be detrimental to gait stability since forward motion relies on three legs forming a tripod.

Myriapods have a morphology consisting of a flexible, elongated, and segmented body with many legs that gives them a comparative advantage in certain terrains and situations relative to other arthropods. One group of myriapods that has captured attention of the engineering community is the Chilopoda, commonly known as centipedes [8–11]. As pursuit predators, centipede locomotion employs a metachronal gait such that it imparts impressive speed and utilizes body undulations to maximize strides [12, 13], which is generally limited to surface activity and not subterranean burrowing. Another myriapod group commonly known as millipedes (class Diplopoda), has been less investigated in engineering literature.

Despite having morphology similar to that of centipedes, there are distinct differences that makes millipede locomotion intriguing for robotic applications. Millipedes are detritivores, which do not chase prey but navigate through the forest floor, burrow into leaf litter, dead wood, and soil. Therefore, the locomotion requires not only handling surface activity on uneven terrains, but also a powerful gait capable of handling resistive loads introduced by burrowing. To accomplish effective burrowing, the millipede exoskeleton and musculature does not utilize body compression, rather it relies on a gait that does not impart body undulations as observed for centipedes. A visual comparison of these two myriapod metachronal gaits is shown in figures S1A and S1B (https://stacks.iop.org/BB/16/026003/mmedia).

There are limited number of studies on general myriapod locomotion, whether via simulation model or robotics. Prior literature [14–20] has primarily focused on the decentralized control schemes of a myriapodous platform utilizing feedback to generate a responsive gait behavior. A preliminary experimental investigation [21] on millipede-specific locomotory mechanisms for traversing complex terrains has revealed that: (i) millipedes possess segments along their body that moves relative to each other with three degrees-of-freedom in a sequential manner to smoothly transition into the given direction of motion, and (ii) there is a metachronal gait which results in a traveling wave that can be modulated on surfaces with different resistances (figures 1(E), (F) and S2). These findings were consistent with the initial study performed by Manton [22] that demonstrated traveling wave modulation for varying thrust force performance. It is worth noting that the observed wave form is modulated such that it maximizes the number of anchoring points. This observation differs from the approach used in literature for modeling traveling wave locomotion ([23, 24]), where assumption is often made that the waveform is unclipped sine wave.

In this study, the locomotion mechanisms utilized by millipedes are investigated to reveal the fundamental principles that impart traveling wave created by the aggregate leg motions that can resist significant loading. Two complementary approaches were used: (i) experimental observation from two live species of millipede walking against pre-determined loads and (ii) measuring the thrust force from a biomimetic robotic platform designed to emulate the gait behaviors and use the measured data to validate the developed model. Through combination of dynamic simulations and experimental observations, we reveal how the millipedes locomotion naturally overcomes resistive forces and why such multi-legged morphologies are advantageous. Fundamental understanding of locomotion principles achieved through these models and experiments was tested on a robotic platform and the results demonstrated an expected increase in the thrust force.

The paper is organized in three sections: experimental results and observations, discussion and conclusion, and materials and methods. These sections are organized in such as way that allows answering questions of increasing complexity.

2. Experimental results and observations

This section starts with a discussion on the live millipede experiments and initial observations. The next subsections relate to modeling, gait and morphological analysis, and robotic platform. Collectively, the information from these subsections provides answer to the following questions: i) can we develop a model to determine the thrust force with a single input? ii) What factors dictate the other behavioral variables? iii) Why do millipedes prefer a certain range of duty cycles? iv) Why do they have so many legs? And v) can we emulate their gait for high thrust on a robot?

2.1. Live millipede experiments

In order to perform the experimental studies on live millipedes, two different methods were used. First, the slope of a preset walkway was incrementally increased to control the resistive force (behavioral response) acting against the millipedes' motion. The slope was varied over a wide range of angles (0°–50°) to determine the relationship of the traveling wave modulations with the forward thrust (figure S3A, video S1). Second, a novel stage was designed to emulate the varying burrowing environments. The stage exerted loads axially and radially on the millipede body and the resulting gait adjustments were recorded (figures 1(G), (H), S3B, video S2).

The live experiments were performed using two species of millipedes that encompass two of the four burrowing ectomorphs in Diplopoda. The first, *Apheloria virginiensis* (figure 1(F)), are considered flat-back millipedes (polydesmida) that grow to a length of approximately 5 cm with a total of thirty leg pairs. They use a 'wedging' burrowing technique, which involves inserting the anterior (head) end by lowering it into a narrow crevice or crack and then widening the gap by pushing up with their legs and straightening their body (elevating their head) [25]. The second, *Narceus americanus* (figure 1(E)), are nearly cylindrical in shape (juliform) and grow to about 10 cm in length and possess over 80 leg pairs. With such a body structure they are known to employ a 'bulldozing' burrowing technique by ramming their heads into the substrate [25], resulting in less vertical movement of the anterior end. Further details on the experimental setups and specimens can be found in the 'methods' section.

The most notable locomotion characteristics found in live animal experiments are the traveling

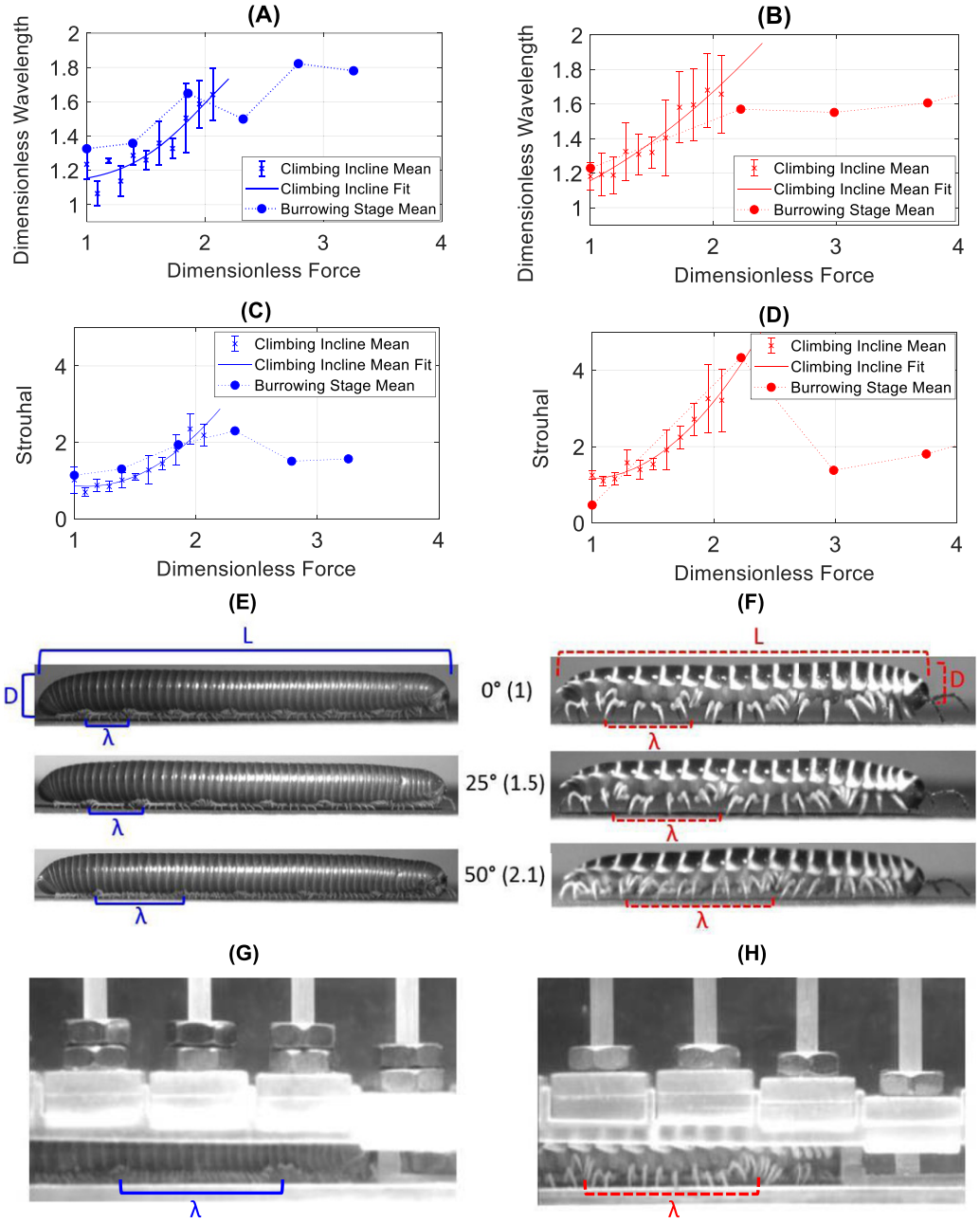

Figure 1. The top two figures are a comparison of results from the incline stage and burrowing stage experiments of the relationship between dimensionless wavelength and dimensionless force of (A) *Narceus. americanus* and (B) *Apheloria. virginiensis*. The second row of figures does a similar comparison from the two experiments, but looking at the relationship between the Strouhal number and dimensionless force of both species (C) *N. americanus* and (D) *A. virginiensis*. These comparisons between the incline stage and burrowing stage experiments indicate that the same gait adjustment is made regardless of the means in which resistance is encountered. The third row of figures are sample images of three different cases used to determine the wavelength on the incline stage for (E) *N. americanus* and (F) *A. virginiensis*. The bottom row are images of both species crawling in the burrowing stage (G) *N. americanus* and (H) *A. virginiensis*. Note that λ is wavelength.

wavelength and velocity resulting from the aggregate behavior of the legs. To compare between different species moving at different speeds, dimensionless parameters for representative of force, wavelength (measured peak-to-peak as shown in Figures 1(E)–(H), as position of the highest elevated leg) and wave velocity (measured as the velocity of peak or highest elevated leg) were used. The dimensionless force is the resistive force as a ratio of the specimens' body weight. The dimensionless wavelength (λ_{DL}) was calculated using equation (1):

$$\lambda_{DL} = \left(\frac{\lambda}{L}\right)\left(\frac{DN}{L}\right), \tag{1}$$

where λ is the actual wavelength, L is the body length of the millipede specimen, D is the body diameter (shown in figures 1(E) and (F)), and N is the number of leg pairs. The first component captures the length ratio of the generated traveling wave with the length of the specimens' body. However, this

calculation alone does not make the locomotion characteristics comparable between different millipede species given the wide variation in morphologies. The multiplied dimensionless number captures these different features by an aspect ratio of the body and the number of leg pairs (proportional to number of active body segments). These parameters were selected based on the Manton's [22] observation that the force output from the millipedes' muscles is proportional to its body segment or ring volume (note that a body segment is characterized by lengths D and L/N). This permitted us to draw comparisons in wave modulation across the two different species despite the differences in size and morphology. To compare wave velocities, the effective Strouhal number was determined for each case. While typically used for fluid dynamic applications, the Strouhal number is the ratio of the wave velocity to the body velocity, which provides a dimensionless value to compare the locomotion cases.

Inclination Experiment:

Wavelength—Consistent with previous findings [21, 22], there is a clear increase in wavelength with increased propulsive force demand as shown in figures 1(A) and (B). In these figures, there is a distinct increasing trend in dimensionless wavelength for both species climbing steep inclined surfaces. It is notable that all specimens refused to climb on the given surface at the angle that emulated a resistive force just over twice their weight. An increase in wavelength is a result of adjusting the number of legs per wave, but doing so while maintaining a 'constancy in forward strokes' [22]. This results in a higher ratio of legs in the propulsive backward stroke phase to the swinging forward stroke phase per wave. The generated wave form undergoes a mechanically clipped deformation of a sinusoidal wave increasing both in length and amplitude (figure S6D). Assuming that all the legs are performing identical motions [21, 22, 26], with only slight variation in phase, the motion will be indicative of an increase in duty cycle (the quotient of stance duration and stride duration) with increasing resistive force (also referred to as 'duty factor'). In other words, the resulting quotient of legs in the stance per wave (or across the entire body) is also equal to the duty cycle of an individual leg. The duty cycle varied between 0.3 and 0.7, as seen in figure 2(C), which will be discussed further in modeling and analysis sections.

Wave velocity—While it was observed that the wavelength was not significantly adjusted by variations in body speed, the wave velocity was certainly influenced as it directly relates to the motion of the legs. We found a clear correlation of the Strouhal number with increased dimensionless force for both species, as shown in figures 1(C) and (D). While the wave velocity and duty cycle are independent variables, they become related when the velocity of the elevated legs performing forward strokes is held constant but the velocity of legs in backward stroke slows down. In terms of the Strouhal factors, the wave velocity following the concept of 'constancy in forward strokes' [22] not only holds for number of legs elevated, but the movement as well, while the velocity of the body decreases. As a result the wave velocity (thus Strouhal number) is directly related to the duty cycle [26], which increases in order to create the change in wavelength.

Burrowing Experiment:

Wavelength—To determine if the behavioral response of the millipedes during the climbing incline experiments translates to burrowing applications, the initial tests were performed with only a horizontal (axial) resistance present in the burrowing stage. In figure 1(A) and (B), the wavelength adjustments made by both species, in cases of only horizontal (axial) resistances, follow the similar trend that the millipedes exhibited in the climbing incline experiment. This trend is observed up to the resistance value after which the millipedes refused to climb. Beyond that threshold, the millipedes still exhibited capabilities of burrowing, however, the adjustments in gait behavior shifted and becomes sporadic. Trials were performed by introducing combinations of horizontal (axial) with vertical (radial) loads, and while the changes in gait are sporadic, there still exists an increasing trend of the wavelength, as seen in figures S5A and S5B. Note that the load increments on the burrowing stage were the same for both species. Thus, while the *N. americanus* was willing to burrow through all combinations of axial and radial resistive loads, the *A. virginiensis*, which is considerably smaller (about half the length and weight) and a different ectomorph, refused the burrowing under higher loads.

Wave velocity—The wave velocity created by the metachronal gait while in the burrowing stage against only horizontal (axial) loads, follows the same trend as displayed in the incline experiment up to about twice their body weight, as shown in figure 1C and (D). Beyond this load limit and introduction of vertical (radial) loads, the adjustment in wave velocity, like that of wavelength, becomes sporadic. From the results of these two experiments, we find that the incline experiment captures the behavioral gait adjustment response with regards to horizontal (axial) loading. This allows us to utilize the fine incremental control of the incline experiments to understand the changes in millipede locomotion dynamics when encountering loads against the desired direction of motion.

2.2. Gait dynamic model

Kinematic studies have been conducted in literature to determine the position and motion of millipede legs to create a traveling wave [21, 26]. However, prior models lack the dynamics of the gait. Fang *et al* [14]

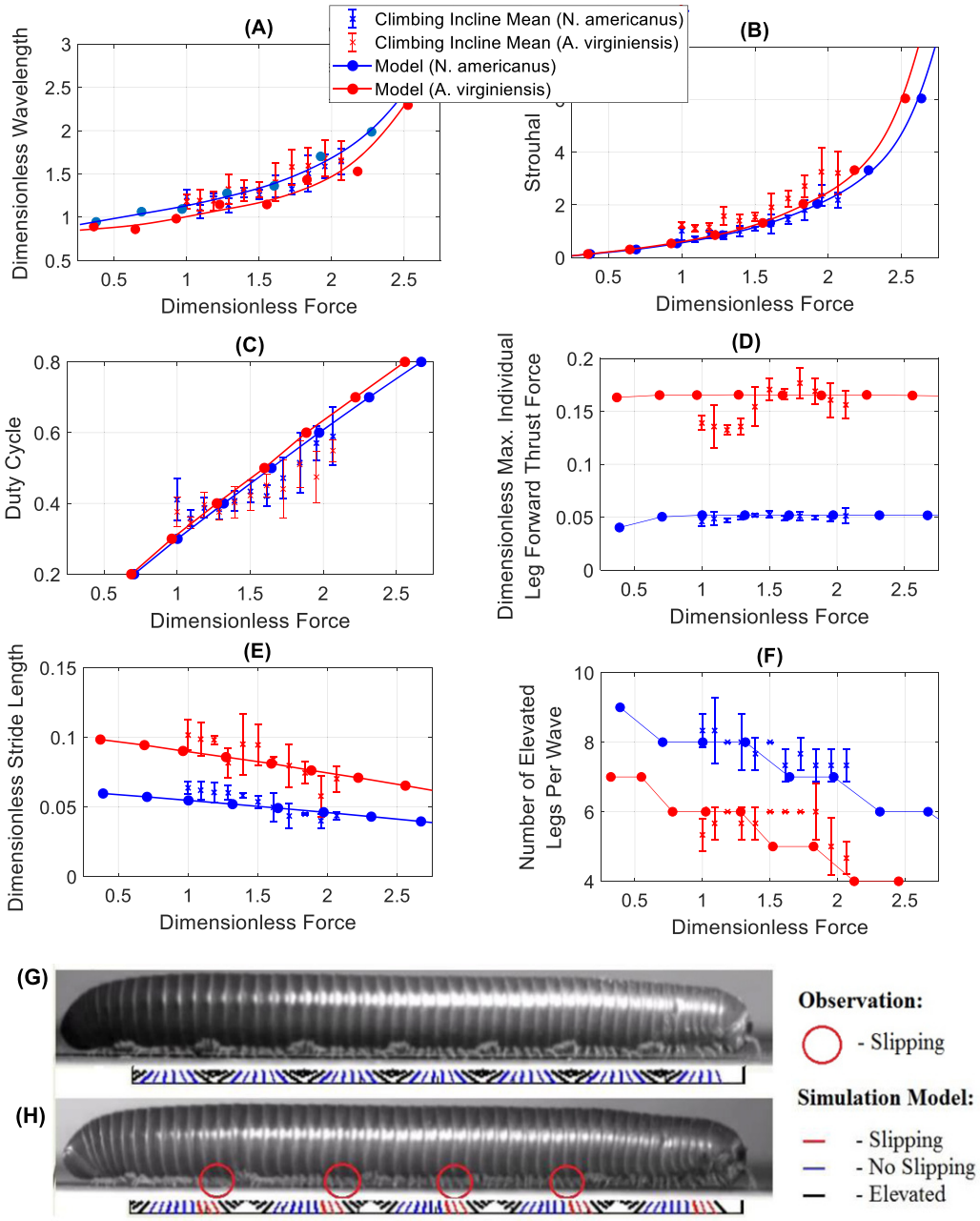

Figure 2. These plots compare the experimental results of both millipede species in the incline experiment with results generated by the simulation model: (A) dimensionless wavelength versus dimensionless force, (B) Strouhal number versus dimensionless force, (C) duty cycle versus dimensionless force, (D) leg thrust force versus dimensionless force, (E) dimensionless stride length versus dimensionless force, and (F) legs elevated versus dimensionless force. The bottom two figures show a comparison of the experimentally observed *N. americanus* with the simulation model of leg behavior below, where black legs are elevated, blue legs are in contact with the ground, and red legs are slipping: (G) experimental observation compared to model with no slipping (H) experimental observation compared to model with slipping.

used the deformation of elastic meshes to determine external reaction forces applied to rigid bodies. Siddall [27] explored a simpler approach to determine the forces involved in a metachronal gait system, taking a quasi-static approach (equations S1–S4). The model assumed a many legged robot body with pneumatic cylinder legs that could autonomously adjust in length, with forces transmitted by a single rotating degree of freedom. The resulting forces were calculated by summing up contributions attributed by weight and rotation at the hip using trigonometric functions of sine and cosine determined from the angle of the legs.

Building upon these kinematic [21, 26] and dynamic [27] models (figure S6 and table S3), simulations were developed to emulate the walking mechanics of millipedes'. In this model, both morphological and behavioral variables were considered. Morphological variables included the body length, number of body segments, number of leg pairs, body diameter, and leg length. Behavioral gait variables included duty cycle, stride length, leg thrust force, velocity, and

phase difference. In the initial modeling process, average values of morphological features were selected for both species, as shown in tables S1 and S2. The morphology assumes two leg pairs per body segment, and additional weight on the anterior and posterior ends of the body corresponding to the section of the animal body ends that do not possess legs. To determine the relationships of parameters with the overall thrust force, the behavioral gait variables were measured from the incline experiments and applied in the model.

2.2.1. Development of a model to determine the thrust force a millipede generates using a single behavioral input

From the experimental results, a dominant observation was the change in duty cycle, and therefore this variable was used as the model input. The duty cycle range was 0.3 to 0.7 for both species (figure 2(C)). The other behavioral variables that could be observed were the stride length and the phase between leg pairs. The stride length slightly declined with increasing thrust force (figure 2(E)), while the phase, which dictates the number of legs elevated per wave (Manton [22] described it as 'constancy in forward strokes'), appears to slightly decrease as well (figure 2(F)). The final variable of interest was the force output of an individual leg, but unobservable. To estimate the force output, the other behavioral variables experimentally measured for each specimen were used to generate kinematic simulations for determining the leg positions through time. Knowing the leg positions/angles, the force values of each leg were back calculated using the quasi-static approach proposed by Siddall [27] (equations S1–S4). However, comparing the simulation with observation, there was discrepancy with expected slipping behavior (figure 2(G) and (H)). The model determined slipping would occur on legs during the latter half of the propulsion stance, just prior to elevating the leg. On the other hand, observation of the actual specimens suggested that the contrary was true, such that majority of the slipping occurred during the initial half of the propulsion stance just after landing. Given that the friction force tangential to the surface determines if a leg experiences slipping, the magnitude of the normal ground reaction forces become the governing factor (assuming a constant coefficient of friction).

In the simulation, these forces were calculated based on the assumption that the force driving the leg consisted of only a single degree of freedom, resembling torque applied to a pendulum. Actual millipede legs have multiple degrees of freedom that can influence the ground reaction forces during the propulsive stage. Further model development was required considering these other degrees of freedom, but without redundant complexities (figure S8). The quasi-static model was modified such that limited vertical force is applied initially after landing, then gradually increases until mid-stance, and afterwards provides relatively large forces pushing the body forward until the leg is elevated for the forward stroke. Such fine control is not unreasonable considering the complexity of their musculoskeletal system and central nervous system [28] (figure S9). Mathematically in the model, the propulsive normal force action was initially driven by a single degree of freedom, where $F_{PN} = K \sin\theta$ (K is a coefficient proportional to segment weight), and it was later modified to $F_{PN} = K(\cos\theta - \sin\theta)$. A visual comparison of the implemented change to the dynamic model of the propulsive force is shown in figure S8D. This adjustment to the simulation captures the slipping behavior observed (figures 2(G) and (H), video S4 and S5). Furthermore, the model indicates that the maximum force on an individual leg stays relatively constant regardless of the overall thrust force demand for the body. This shows that the ability to improve thrust force is not dependent on the increasing effort of the legs, but primarily on the gait pattern used (figure 2(D)). The variation in effort by an individual leg is more in the *A. virginiensis* compared to the *N. americanus*, which could be related to the fact that the *N. americanus* has more legs, permitting finer control over the traveling wave gait modulations and less dependency on individual leg effort.

2.2.2. Factors that dictate behavioral variables of stride length and legs elevated per wave (leg phase difference)

Taking the dominant factor, duty cycle, as the input the behavioral parameters that further need to be modeled are the stride length and number of legs elevated per wave. Sweeps were performed for varying (physically possible, limited by maximum leg length) values for each stride length and number of legs elevated, while holding the other variables constant. The variations in stride length revealed small changes in total thrust force of the gait, which is negligible relative to the change in total force created by adjustments in duty cycle. The modeling approach for stride length used was a linear scaling of the leg length between the largest to smallest strides observed (figure 2(E)). The changes made in number of legs elevated per wave, did not affect the overall thrust force of the gait. The 'constancy in forward strokes' (Manton [22]) results in more legs in contact with the ground per wave as the wavelength is increased. However, changing the number of legs elevated the 'constancy in forward strokes' profile per wave but does not change the ratio of number of legs in contact with ground across a single wave, or the entire body, if duty cycle is maintained. In other words, for a given duty cycle, more legs elevated would result in a longer wavelength with more legs in contact with the ground. In order to model the number of legs elevated per wave, the main issues to address are (similar to those that Manton [22] encountered): (i) if there are too many legs

elevated per wave, it would result in a large region of the body without vertical support, thereby, forcing dependence on the musculature between body segments to hold adjacent segments off the ground (figure S10A); (ii) if there are too many legs elevated (for a given duty cycle), the phase difference between leg pairs decreases, resulting in an increase in wavelength. Too large of a wavelength would result in instability (figure S10B); (iii) if there are too few legs elevated off the ground, this would lead to overcrowding between leg pairs in the propulsive stance (figure S10C).

Given these issues, it is expected that the millipede minimizes the number of legs elevated and maximizes the number of legs in contact with the ground for both support and propulsive purposes. The sensory feedback mechanisms involved in this process is beyond the scope of this work, but may relate to the mechanisms explored in literature [15, 16, 20]. With this premise, the number of legs elevated is minimized, but with avoidance of overcrowding of legs in the propulsive stance. Considering that the stride length shows an inverse trend, the following relationship was generated:

$$N_{\text{LegsElevated}} = \left(\frac{2S}{d}\right), \tag{2}$$

where $N_{\text{LegsElevated}}$ is the number of legs elevated per wave, S is the stride length, and d is the distance between leg pairs. This equation is illustrated in figure S10D. If the numerator in equation (2) was just a single stride length, it will indicate that there would be a collision between leg pairs in contact with the ground (leg just prior to elevating and leg that just landed). This implies any slip on the surface could potentially cause one leg tripping. If there was an instantaneous demand for vertical support of the body segments with elevated legs, there would be no space in between the legs performing strides for the elevated legs to fall. The gap of another stride length maintains the gap where legs are elevated minimally but provides enough space to avoid collisions due to overcrowding. Using this relationship, the model matches the observation with regards to the number of legs elevated per wave (figure 2(F)).

From experimental observations, we constructed a model, which based upon the morphology of the millipede specimen, can determine the mechanics of the metachronal gait as well as the traveling wave locomotion characteristics of wavelength and wave velocity (figure 2(A) and (B)) with the corresponding output thrust force.

2.3. Millipede gait and morphological analysis

We modeled the millipedes' primary mechanism of gait adjustment to handle increased resistive loads, which appears to range from its own body weight to just over twice its weight. In refining the model, we tested the behavioral parameters that includes duty cycle, stride length, phase difference, and their effects on the overall performance regarding thrust force. We also found that the individual leg force stays constant (at least within the desirable behavior exhibited from the experiments). It became evident from the modeling results that the duty cycle was the primary factor in changing forward thrust. We found that the millipedes keep the wavelength as short as possible to avoid instability. They also maintain 'legs elevated profile' as small as possible to maintain upright support across body segments. Note that this resulting wave form is a clipped sinusoidal wave increasing not only in length, but in amplitude as well (figure S6D), unlike existing traveling wave locomotion approaches found in literature [23, 24, 29, 30]. We have addressed the behavioral variables of stride length and phase difference (number of legs elevated) in our development of the simulation model, however, the behavior of duty cycle has been treated this far as the input to our system. What dictates the duty cycle has yet to be determined.

2.3.1. Optimum duty cycle range for millipedes

It is interesting question that why the duty cycle is in the range of 0.3 and 0.7. For the thrust force capabilities, the larger duty cycle is preferred. However, the cost of a high force duty cycle is the decrease in velocity of the leg during the stance phase propelling the body forward. This can be demonstrated by determining the cost of transport (COT) through equation (3):

$$\text{COT} = \frac{P_{\text{input}}}{WV_{\text{body}}}, \tag{3}$$

where P_{input} is the input power provided by the millipede, W is the weight, and V_{body} is the resulting velocity of the millipedes' body. As seen in equation (3), the COT increases with decrease in velocity, which is a result of increasing thrust force by duty cycle. The P_{input} was determined by back calculating the COT value of a myriapod of similar mass as the *N. americanus* [31]. The model was used to calculate the V_{body} for duty cycles ranging from 0.1 to 0.9 (increments of 0.1). Figure 5(F) shows that this behavior of walking with the duty cycle between 0.3 and 0.7 (indicated by o's), operates in the region of COT that is consistent with other terrestrial animals. Walking below a duty cycle of 0.3 (indicated by *x*'s) would likely require larger thrust forces than desired by an individual leg to propel the body forward. While walking at duty cycles greater than 0.7, leads to increase in COT (indicated by *x*'s). Lastly, growing larger and increasing the body mass, does not significantly influence the cost of transport but would make the millipede deviate from the mass-specific energy per unit distance found commonly in terrestrial animals.

In these prior sections, we have addressed how the behavioral gait variables are determined by comparing the model with the experimental observations. However the model has used only the morphological parameters of the observed species. With this model

we can perform a parametric study, to answer why millipedes are so long with many legs.

2.3.2. Why do millipedes have so many legs? Why do the number of leg pairs differ between species?

A parameter sweep from five body segments to 100 body segments was performed by changing the gait variables (duty cycle, stride length, and legs elevated) to see if their influence on the resulting output thrust force was sensitive to the change in the morphological parameter of number of body segments. The surface plots in figure 3 show the results of the sweep using the average segment size of the *N. americanus*. Similar sweeps were also done with the average segment parameters of the *A. virginiensis*, as well as arbitrary segment sizes, by dividing across a fixed body length. Each of these analyses revealed similar trends. Figures 3(A) and (B) show the relationships between wavelength and Strouhal number with changes in number of body segments/legs. While the Strouhal number is not influenced significantly, the dimensionless wavelength is changed. Changing the number of body segments directly changes the body length, and thus the dimensionless wavelength (equation (1)). Figure 3(A) indicates that reducing the number of body segments results in increasing the dimensionless wavelength, which could lead to stability issues. This may suggest that the morphology of body length dictates the behavioral gait limits. In figure 3(C) we can see an increasing total output thrust force with increased number of body segments, however, ultimately with diminishing returns regardless of the duty cycle. Similarly, from plots in figures 3(D) and (E), we can see the asymptotic behavior with increased number of body segments with stride length and legs elevated per wave. These plots confirm the limited influence that stride length and phase difference have on the total output thrust force compared to the duty cycle.

From the model and parametric analysis, it appears that the primary factors that govern the thrust force capabilities of millipedes are number of body segments (morphology) and the duty cycle (behavior). Regarding the number of body segments, from figure 3(C), the asymptotic behavior of the diminishing returns of thrust force per added body segment is found. Given that the weight of each segment stays constant and the thrust force efforts of each leg is also constant, it is unclear that the relationship between thrust output and the number of body segments is not linear. The cause of the asymptotic relationship is the weight of the anterior and posterior ends of the body that do not possess legs to assist with thrust. Disregarding the weight of the head and posterior results in a linear relationship between number of segments and thrust output (constant with dimensionless force), which the actual performance asymptotically approaches as shown in figure 4(C) and figure 4(G). The extra weight governs the rate of the increase in thrust force provided per added body segment. It was noticed that for the *N. americanus*, the anterior and posterior ends of the body are relatively large compared to a single body segment. From figure 4(B), these end segments are equivalent to approximately three body segments each. For the *A. virginiensis*, the anterior and posterior ends are equivalent to the size of a single segment (figure 4(F)). Taking this into account in the models, it was observed that the ratio of the dimensionless force value with the asymptotic value results in a desired minimum number of body segments. For both species, the number of active (with legs) body segments stop at a thrust force, approximately 0.88 ($\approx 90\%$) of the asymptotic value. While certainly being longer provides more forward thrust capabilities, the overall system experiences diminishing returns for the added segments. Furthermore, the price of growing too large may not be biologically advantageous in terms of surviving and escaping predators.

2.4. Millipede robot design, experiments, and analysis

2.4.1. Emulation of the millipede gait to adjust thrust force

To test the conclusions from this model regarding the primary factors in millipede gait and morphology, a millipede-mimicking robot was designed to emulate the metachronal gait. Prior myriapod robots (such as [15–18]) have focused on decentralized control with implementation of feedback sensors. For the robot developed in this study, such complexity is not required. With each leg providing the same effort regardless of the total thrust output, the control scheme can be reduced to controlling the duty cycle. For the legs, a mechanism similar to that found in the model of Wan *et al* [32] was used. This model generates a trajectory consisting of a circular arc and a straight line using a single motor actuator, thereby allowing explicit control of the leg elevated and propulsion stances (Figure S11). This motion is consistent with the actual millipede leg motion previously reported in literature [21]. A detailed account of the millipede robots' component design, controls, and fabrication can be found in the SI (figures S11 and 12). A single millipede robot segment and assembly of five segments is shown in figure 5(A) and (B). With explicit control of the individual leg propulsion and elevated stances, the ranges of gaits exhibited by the millipede could be emulated, essentially modulating the traveling wave locomotion (shown in figure 5(B)).

Our goal here is to understand how variation in gait behavior and body morphology affects thrust force capabilities. For this experiment, the gait pattern is the input (duty cycle) to the robot system of a certain morphology (number of body segments) and the thrust force from the robots' locomotion is directly measured using the setup shown in figure S13. The

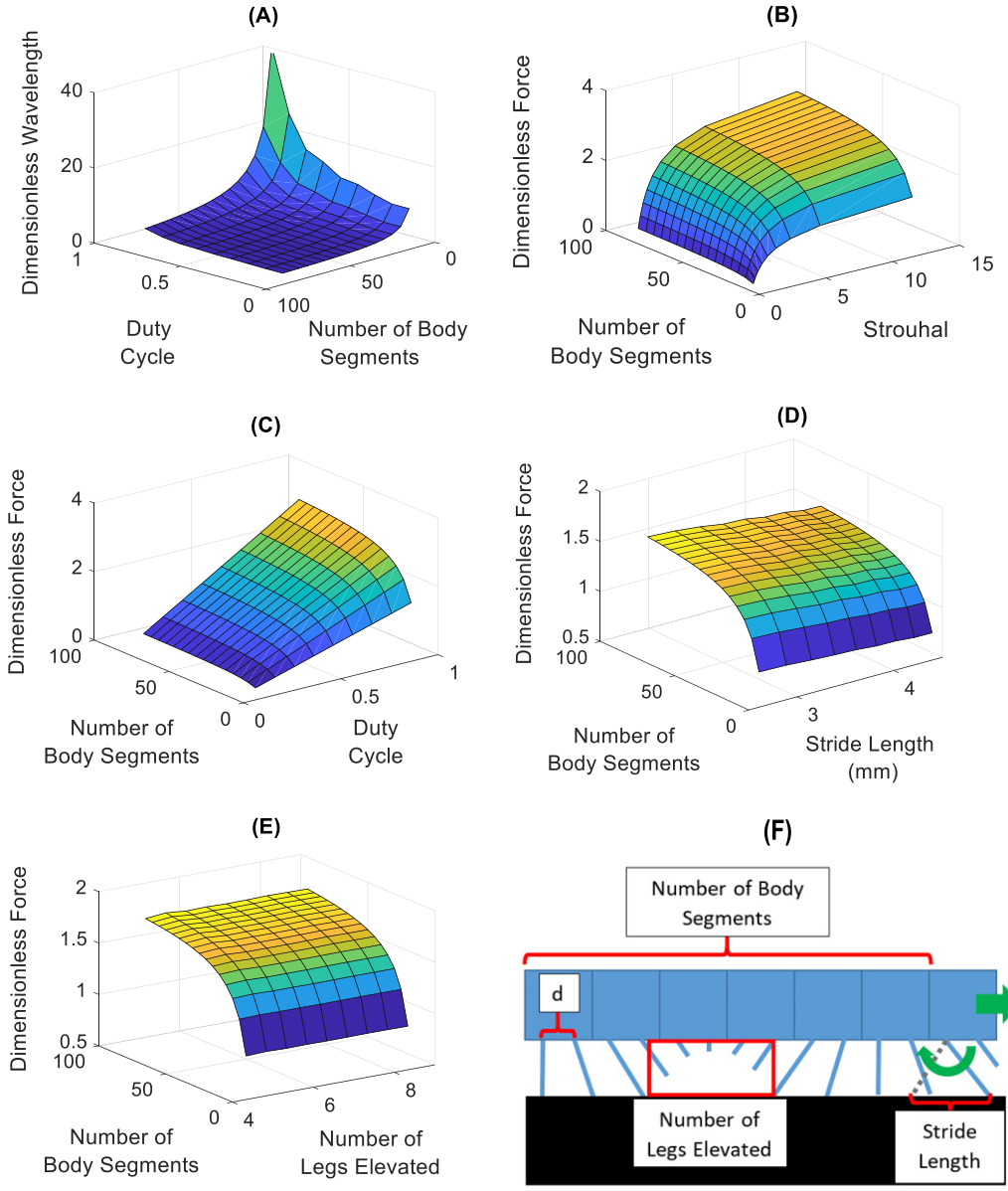

Figure 3. The following surface plots are those of a millipede possessing the body segment parameters of a *N. americanus*. The first row of plots provide (A) dimensionless wavelength vs duty cycle vs number of segments and (B) dimensionless force vs strouhal vs number of segments. The next three surface plots provide the relationships of dimensionless force vs number of segments vs the three main behavioral variables (C) duty cycle, (D) stride length, and (E) number of elevated legs. Note that for plots (C)–(E) the other behavioral variables are held constant. Figure (F) illustrates of parameters being analyzed and used in equation (2).

robot pulls on a fixed load cell while crawling on a rough surface (sandpaper) and sliding on the smooth acrylic surface. As a result, the thrust force generated by the propulsive stroke is transmitted to the load cell with the robot held stationary.

The other millipede robots gait variables and morphological features, aside from duty cycle and number of body segments/legs, were maintained constant (equation (2) to determine the temporal phase difference). Using these robot parameters (table S4), a model representation of the robot was simulated. Notably, that the robot did not possess extra segments or body weight beyond the locomotive segments, as a result, the dimensionless force (thrust force as a ratio of the body weight) did not display any asymptotic behavior, analogous to the linear plots in figures 4(C) and (G). The results of the millipede robot were found to be consistent with the dynamic model predictions, as shown in figures 5(C) and (D). Being able to emulate the model predictions with the robot suggests that the extracted conclusions on millipede behavior and morphology related to their effects on forward thrust force abilities are substantial.

With the model, we sought to determine the desirable length of the millipede robot. However, without the asymptotic behavior observed with the biological millipedes in figures 4(C) and (G), the optimal body length for the robot could not be attained from the same approach of comparing the curve with legless segments to the case without legless segments.

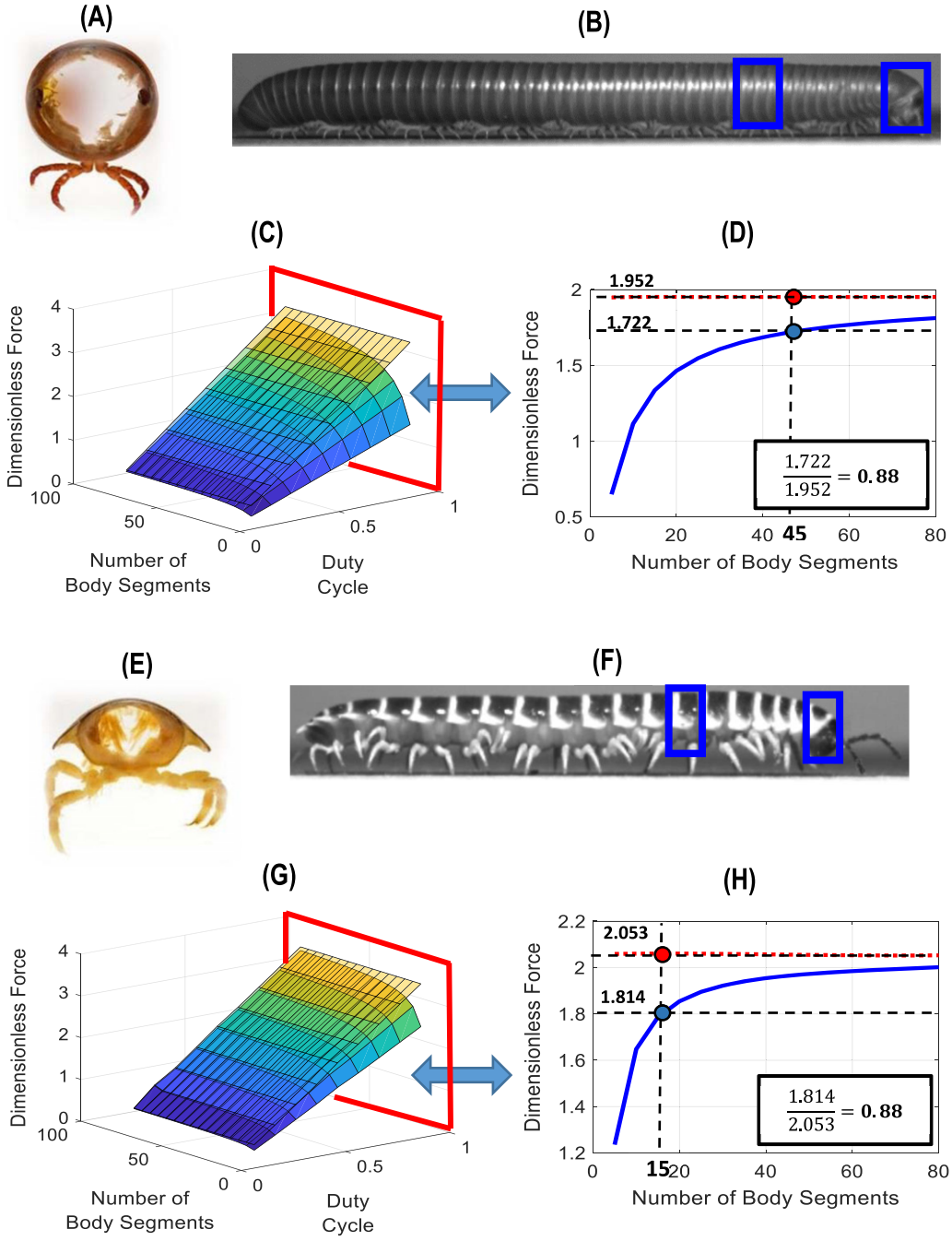

Figure 4. These sets of figures illustrate the influence of body length (by changing the number of body segments) on thrust force for both species. The top box shows results for the *N. americanus* (A) the anatomy of single body segment (B) a comparison of the approximate size of body ends without legs to individual body segments (C) surface plot of dimensionless force vs number of segments vs duty cycle (linear plot disregards weight of legless anterior and posterior ends) (D) plot of dimensionless force vs number of segments at a duty cycle of 0.5 (red line disregards weight of legless anterior and posterior ends). The bottom box shows for the *A. virginiensis* (E) the anatomy of single body segment (F) a comparison of the approximate size of body ends without legs to individual body segments (G) surface plot of dimensionless force vs number of segments vs duty cycle (linear plot disregards weight of legless anterior and posterior ends) (H) plot of dimensionless force vs number of segments at a duty cycle of 0.5 (Red line disregards weight of legless anterior and posterior ends).

Another approach for determining the optimal number of body segments for the robot is using the desired duty cycle behavior and dimensionless wavelength. Given the dimensions of the robot segments, and duty cycle range of 0.3 to 0.7, the range of corresponding wavelengths can be determined. With the known wavelengths from the robot, we can determine the ideal robot body length by comparing the dimensionless wavelengths observed on the biological millipedes. The dimensionless wavelength defined in equation (1) was entirely determined from the geometry of the millipedes. The equation took inspiration from Manton's [22] revelation that the volume of the body segment was proportional to the leg musculature, and thus effort capabilities. Comparing biological specimens, the second factor in equation (1)

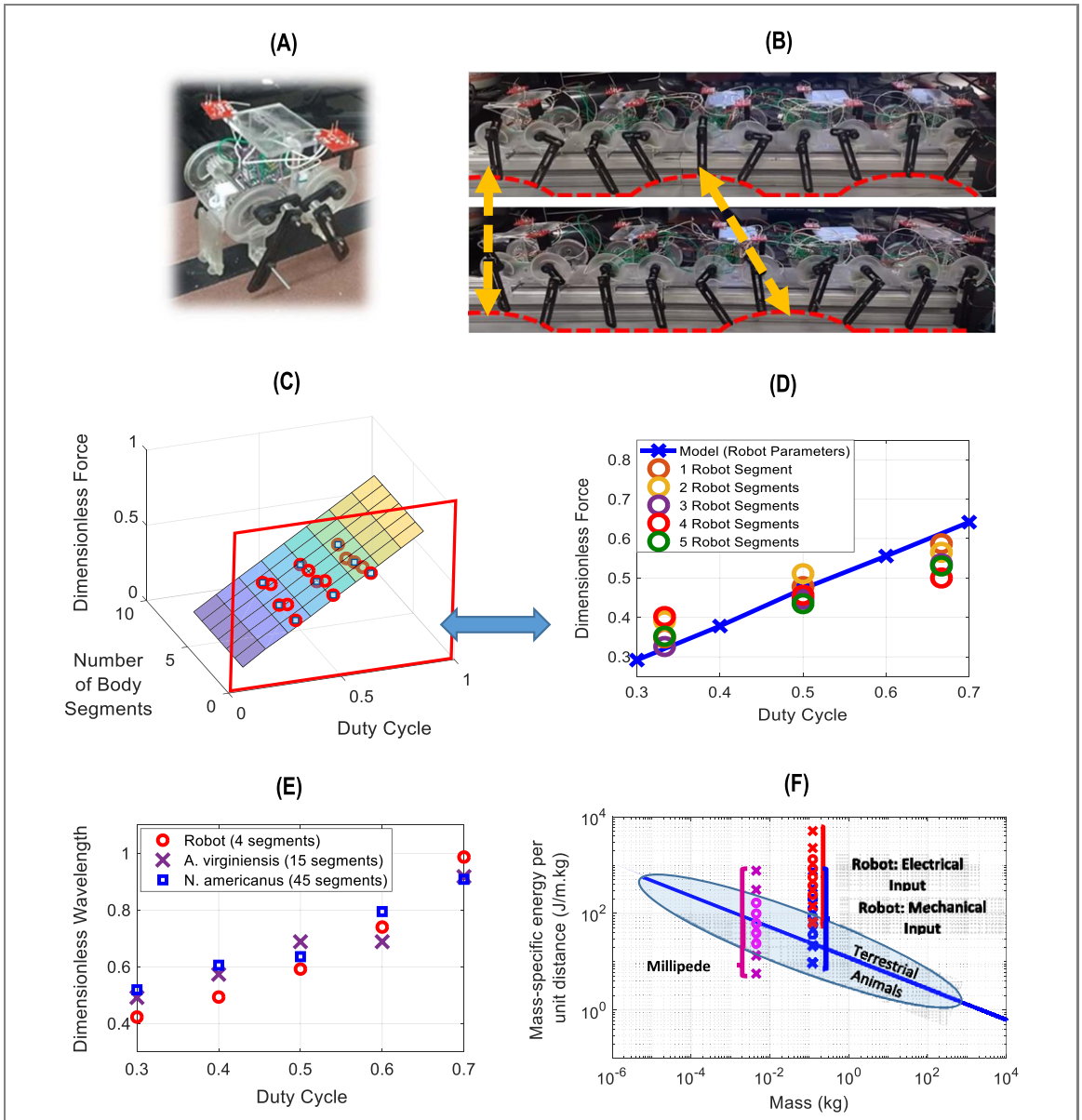

Figure 5. The top two figures are pictures of the millipede robot: (A) is the assembly of a single body segment, and (B) is a full body consisting of five segments performing gaits with 0.3 and 0.7 duty cycle, illustrating the resulting change in wavelength, analogous to figure 1(E) and (F) for the live millipedes. The second row of plots show a comparison of the simulation model and the millipede robot: (C) simulation model comparison of dimensionless force vs number of body segments vs duty cycle, and (D) dimensionless force vs duty cycle. Plot (E) compares the updated dimensionless wavelength (equation (4)) of actual millipedes and 4-segmented robot. Figure (F) illustrates the COT of millipede and robot versus terrestrial animals (o–indicate COT using gaits of duty cycles 0.3 to 0.7, x–indicates gaits below 0.3 (bottom) and above 0.7 (top)).

takes an assumption of matching muscular density, permitting the calculation of leg thrust force relative to the body segment weight on body dimensions alone. To prove this assumption, it was found that for both species, the individual leg forward thrust effort was equivalent to twice their body segment weight. In order to make a fair comparison for the robot, the equivalent ratio representative of the body segments and legs muscular force density of the robot needed to be determined. The individual leg thrust force was only 2/3 of the weight of the body segment weight, which is much smaller compared to the biological specimens. To compensate for this difference, the dimensionless wavelength equation was updated to incorporate the segment weight to leg force effort ratio, as shown in equation (4).

$$\lambda_{DL} = \left(\frac{\lambda}{L}\right)\left(\frac{DN}{L}\right)\left(\frac{W_{segment}}{F_{leg}}\right), \qquad (4)$$

where F_{leg} is the maximum forward thrust force of an individual leg and $W_{segment}$ is the weight of a single body segment.

This adjustment to the dimensionless wavelength formulation allows a comparable value taking into consideration the strength of the individual legs relative to the body. Surface plots of the updated dimensionless wavelength versus number of body segments versus duty cycle were generated for segment parameters for both millipede species and the robot. It was found that the updated dimensionless wavelength for

both species, at their average biological lengths, operate approximately between 0.5 and 1, corresponding to the duty cycle range of 0.3 to 0.7. For the robot, the dimensionless wavelength curve has values between the range of around 0.5 and 1, corresponding to a duty cycle range of 0.3 and 0.7, at 4 body segments. A comparison of these dimensionless wavelengths, for the millipedes' actual number of legged body segments, and the robot with 4 segments is shown in figure 5(E).

With the millipede robot morphology and gait, we can also determine the cost of transport for the robot. Given the consistent outcomes between the robot locomotion and model, the model was used to determine the COT. Initially, the power input used to calculate equation (3) was using electrical input into the motors. The resulting COT is seen in red in figure 5(F). However, operating at the angular velocity ranges to perform the desired gaits, the motors were only functioning at approximately 20% efficiency. Taking this into account as the actual mechanical input into the locomotion, the COT transport is seen in blue in figure 5(F). As it can be seen in figure 5(F), the cost of transport for the robot is relatively high compared to the actual millipedes and other biological terrestrial animals. This is likely due to the energy losses not just from the motor, but the robots' mechanisms utilized to achieve locomotion. The higher COT is common in most terrestrial robots [33], as engineering and technology continue to try emulate the efficient locomotion techniques observed in nature.

3. Discussion and conclusion

We have investigated the behavior of millipedes' operating in the desirable space where the temporal phase difference between legs is governed by equation (2) and the individual leg effort remains relatively constant, with the primary variable being the duty cycle. This can be seen in yellow regions in figure 6(A). However, the millipedes demonstrated that they can handle larger thrust force abilities beyond that space, but the observed gait behavior became sporadic despite maintaining the trend of increasing wavelength (green regions in figures 6(A) and (B)). Figure 6(B) is a surface plot of the results of loading in both horizontal and vertical directions in the burrowing stage seen in figures 1(G) and (H). To begin to understand what is occurring, the observed gait at this instance indicated by the X in figure 6(A) was replicated in the model. From the observation of the video footage the temporal phase difference between legs was adjusted as well as the duty cycle. More interestingly, for such a gait to achieve that amount of forward thrust, it was calculated that the individual leg effort needed to increase about 20%. This suggests that the variation in gait behavior for forward thrust in millipedes follows the behavioral pattern shown in figure 6(C). The primary factor is the duty cycle, followed by adjusting phase difference and leg effort. More data is required to support this hypothesis in future works.

This study focused on the fundamental mechanisms that govern millipede locomotion dynamics and morphology. We have performed systematic observation of the variation of gaits of live millipedes of different ectomorphs, developed a dynamic simulation model, and validated our findings on locomotion dynamics and morphology through a millipede robotic platform. In the process we have answered the five questions presented in section 2:

i) Can we develop a model to determine thrust force with a single input?

A quasi-static simulation model was developed for a millipede of specified morphology that utilized an input of duty cycle and determined the resulting thrust force.

ii) What factors dictate the other behavioral variables?

It was determined that the relationship for stride length was a linear scaling of the leg length, and the number of legs elevated (which dictates the phase differences of leg pairs) was governed by equation (2).

iii) Why do millipedes prefer a certain range of duty cycles?

Millipedes prefer to operate with duty cycles between 0.3 and 0.7, as operation outside this range results in undesirable COT.

iv) Why do they have so many legs?

It was revealed that millipedes grow in length (adding body segments each consisting of two leg pairs) to about 90% of the ideal dimensionless force (which is representative of the case of a body without legless body segments), and beyond that there is a diminished return in growing longer.

v) Can we emulate their gait for high thrust on a robot?

A robot was built to emulate the observed millipede gaits and morphology, with results validating our model and findings.

While this work has focused on the primary response of millipedes to increasing thrust force by first adjusting duty cycle, experimental observations and the developed model allowed us to hypothesize secondary and tertiary responses of increased phase difference between leg pairs and increasing individual leg efforts, respectively, to increase thrust forces utilizing locomotion methods operating beyond the desirable cost of transportation.

4. Materials and methods

To characterize how millipedes modulate their traveling wave gait with respect to variations in thrust force

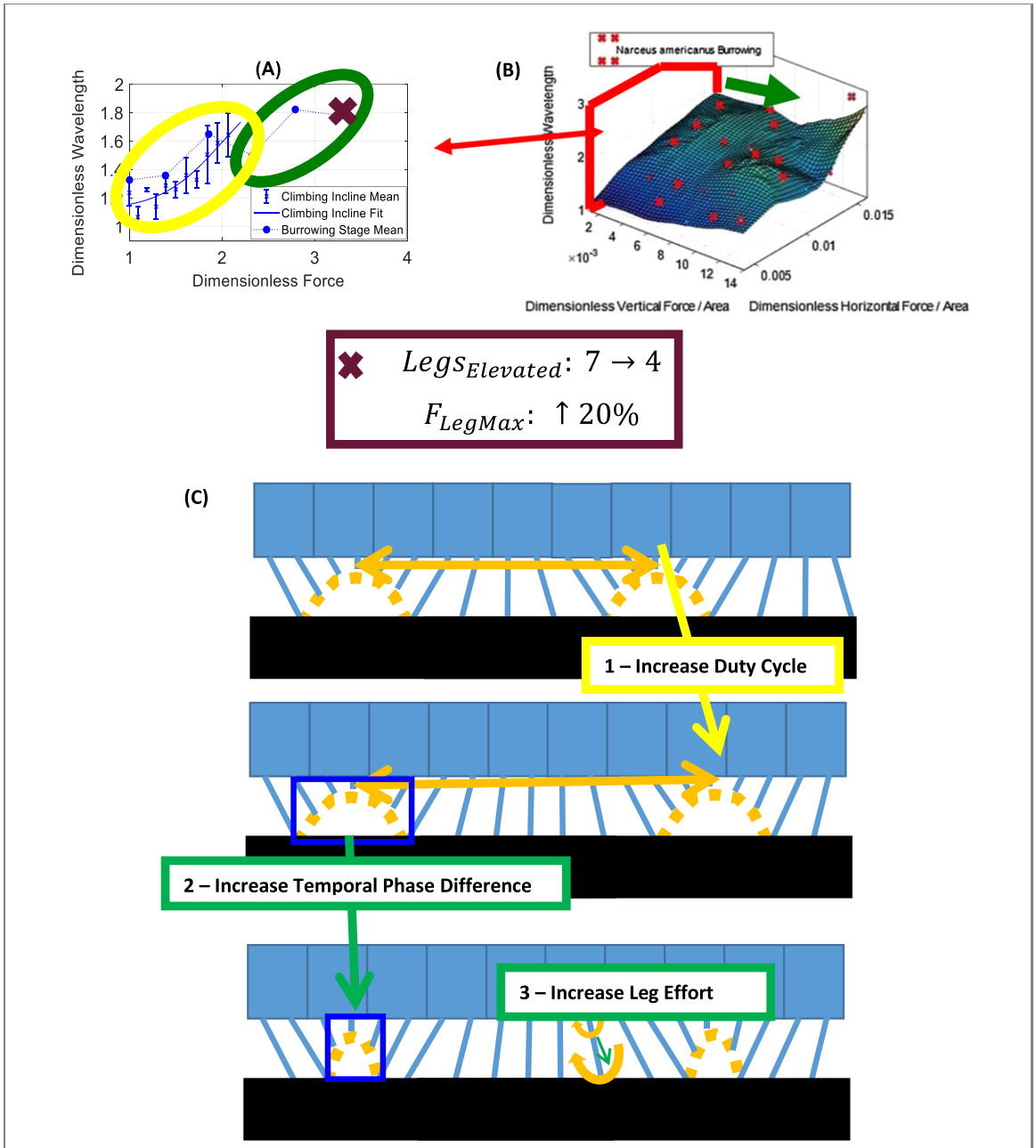

Figure 6. The first row of plots are experimental results of the *N. americanus* in the burrowing stage, showing that they are capable of handling loads greater than twice their weight: (A) *N. americanus* dimensionless wavelength versus dimensionless force (axial loading only), where encircled in green are results of thrust greater than twice their weight. (B) *N. americanus* dimensionless wavelength versus dimensionless force (axial and radial loading), where the green arrow indicates the increase in radial loading. From using the model and emulating the observed gaits in these regions of loads greater than twice their weight, figure (C) illustrates the hypothesized gait behavior adjustment pattern (1) increase in duty cycle (2) reduced number of elevated legs profile (3) increase in individual leg effort.

demand, six specimens (three of each species) were first placed on a ramp, at randomly selected slopes ranging from 0° to 50°, at 5° increments with 15 min rest intervals. Each case was filmed with a high-speed camera operating at 250 fps (Photron FastCam SA4). The ramp stage was controlled with a stepper motor to ensure repeatability of the randomly selected angles (figure S3). The zero position was calibrated with a digital limit switch before each angle adjustment. Sandpaper of 400 grit was placed on the acrylic ramp to allow traction for the millipedes to climb a broad range of angles.

Using the slope to provide a controlled gravitational force in the direction against the desired motion, we quantified the magnitude of the applied force by the millipede. The resisting force caused by gravity is determined knowing the slope angle (F_o) while considering the mechanical and behavioral response due to loss of traction resulting from large incline angles. The effective resistance force (F_R) to motion was determined using the traction on a horizontal case as a baseline, as shown in equation (5).

$$F_R = F_o - (\mu F_N - \mu F_N{}^{0^\circ}), \quad (5)$$

where μ is the coefficient of friction and $F_N{}^{0^\circ}$ is the normal force on the horizontal case.

The second experimental setup also utilized a stage that provided both axially horizontal loads and radially vertical loads. Four specimens were used for this experiment, two *N. americanus* and two *A. virginiensis*. These experiments were conducted to imitate natural conditions of burrowing where the metachronal gait is of importance. The built stage was 3D printed (Objet), and used 8–32 steel screw nuts as weights to incrementally increase the loads in both directions (figures 3(A) and (B)). The same resting time increments were used as the slope experiment and filmed using the same camera settings. The footage was then processed using the open source program DLTdv5 (Direct Linear Transformation digitizing environment) in conjunction with MATLAB to track points of interest. The extracted data was analyzed in MATLAB to characterize the gait.

The millipede robot was tested using the setup in figure S13. The robot thrust performance was directly measured by having the robot pull on a load cell while walking of a high traction sliding surface.

Acknowledgments

The authors acknowledge the financial support from Institute of Critical Technology and Applied Science (ICTAS) and Department of Mechanical Engineering, Virginia Tech. G K acknowledges the financial support from AMRDEC through Center of Energy Harvesting Materials and Systems (CEHMS). S P acknowledges the support from USDA NIFA through award number NIFA-2019-67021-28991. A G acknowledges the support and assistance of Dr. Paul Marek of the Department of Entomology, Virginia Tech.

ORCID iDs

Anthony Garcia https://orcid.org/0000-0002-9464-7109

References

[1] Bachmann R J, Boria F J, Vaidyanathan R, Ifju P G and Quinn R D 2009 A biologically inspired micro-vehicle capable of aerial and terrestrial locomotion *Mech. Mach. Theory* **44** 513–26
[2] Ho T, Choi S and Lee S 2007 Development of a biomimetic quadruped robot *J. Bionic Eng.* **4** 193–9
[3] Fischer G, Gogola M, Garcia E and Goldfarb M 2001 Development of a piezoelectrically-actuated mesoscale robot quadruped *J. Micromechatronics* **1** 205–19
[4] Birkmeyer P, Peterson K and Fearing R S 2009 DASH: a dynamic 16 g hexapedal robot *2009 IEEE/RSJ Int. Conf. on Intelligent Robots and Systems, (IROS)* pp 2683–9
[5] Hoover A M, Steltz E and Fearing R S 2008 RoACH: an autonomous 2.4 g crawling hexapod robot *2008 IEEE/RSJ Int. Conf. on Intelligent Robots and Systems, (IROS)* pp 26–33
[6] Avirovik D and Priya S 2013 Crawling-inspired robot utilizing L-shape piezoelectric actuators *2013 IEEE/ASME Int. Conf. on Advanced Intelligent Mechatronics: Mechatronics for Human Wellbeing, (AIM 2013)* pp 894–9
[7] Avirovik D, Butenhoff B and Priya S 2014 Millipede-inspired locomotion through novel U-shaped piezoelectric motors *Smart Mater. Struct.* **23** 037001
[8] Jimenez B 2007 Centipede Robot Locomotion *Master Thesis* École Polytechnique Fédérale de Lausanne, Lausanne
[9] Koh D, Yang J and Kim S 2010 Centipede robot for uneven terrain exploration: design and experiment of the flexible biomimetic robot mechanism *2010 3rd IEEE RAS and EMBS Int. Conf. on Biomedical Robotics and Biomechatronics, (BioRob 2010)* pp 877–81
[10] Hoffman K L and Hoffma K L 2013 Design and locomotion studies of a miniature centipede-inspired robot
[11] Hoffman K L and Wood R J 2011 Passive undulatory gaits enhance walking in a myriapod millirobot *IEEE Int. Conf. on Intelligent Robots and Systems* pp 1479–86
[12] Manton S M 1952 The evolution of arthropodan locomotory mechanisms: Part 3. The locomotion of chilopoda and pauropoda *J. Linn. Soc. Lond. Zool.* **42** 118–67
[13] Anderson B, Shultz J and Jayne B 1995 Axial kinematics and muscle activity during terrestrial locomotion of the centipede Scolopendra heros *J. Exp. Biol.* **198** 1185–95
[14] Fang J, Jiang C and Terzopoulos D 2013 Modeling and animating myriapoda *Proc. 12th ACM SIGGRAPH/Eurographics Symp. on Computer Animation-SCA'13* p 203
[15] Kano T, Sakai K, Yasui K, Owaki D and Ishiguro A 2017 Decentralized control mechanism underlying interlimb coordination of millipedes *Bioinspir. Biomim.* **12** 036007
[16] Yasui K, Sakai K, Kano T, Owaki D and Ishiguro A 2017 Decentralized control scheme for myriapod robot inspired by adaptive and resilient centipede locomotion *PLoS One* **12** 1–12
[17] Matthey L, Righetti L and Ijspeert A J 2008 Experimental study of limit cycle and chaotic controllers for the locomotion of centipede robots *2008 IEEE/RSJ Int. Conf. Intelligent Robots and Systems (IROS)* pp 1860–5
[18] Tsujita K, Tsuchiya K and Onat A 2001 Decentralized autonomous control of a quadrupedal locomotion robot using oscillators *Artif. Life Robot.* **5** 152–58
[19] Aoi S, Tanaka T, Fujiki S, Funato T, Senda K and Tsuchiya K 2016 Advantage of straight walk instability in turning maneuver of multilegged locomotion: a robotics approach *Sci. Rep.* **6** 3–8
[20] Yasui K, Kano T, Standen E M, Aonuma H, Ijspeert A J and Ishiguro A 2019 Decoding the essential interplay between central and peripheral control in adaptive locomotion of amphibious centipedes *Sci. Rep.* **9** 18288
[21] Garcia A, Priya S and Marek P 2015 Understanding the locomotion and dynamic controls for millipedes: Part 1. Kinematic analysis of millipede movements *ASME Conf. of Smart Materials, Adaptive Structures and Intelligent Systems* pp 1–10
[22] Manton S M 1953 The evolution of arthropodan locomotory mechanisms: Part 4. The structure, habits and evolution of the Diplopoda *J. Linn. Soc. London* **42** 299–368
[23] Spinello D and Fattahi J S 2017 Peristaltic wave locomotion and shape morphing with a millipede inspired system *J. Nonlinear Sci.* **27** 1093–119
[24] Tanaka Y, Ito K, Nakagaki T and Kobayashi R 2012 Mechanics of peristaltic locomotion and role of anchoring *J. R. Soc. Interface* **9** 222–33
[25] Hopkins S and Read H 1992 *The Biology of Millipedes* (Oxford: Oxford University Press)
[26] Sathirapongsasuti J, Punnanithi N and Wimonkittiwat P 2004 A mathematical explanation of millipede's walk: Walking with a Millipede Intel ISEF, Bangkok, Thailand

[27] Siddall J N 1964 The wave mode of walking locomotion *J. Terramechanics* **1** 54–73
[28] Minelli A 2016 Treatise on zoology—anatomy, taxonomy, biology *The Myriapoda* vol 2 (New York: Academic)
[29] Zarrouk D, Mann M, Degani N, Yehuda T, Jarbi N and Hess A 2016 Single actuator wave-like robot (SAW): design, modeling, and experiments *Bioinsp. Biomim.* **11**
[30] Avirovik D, Malladi V V N S, Priya S and Tarazaga P A 2016 Theoretical and experimental correlation of mechanical wave formation on beams *J. Intell. Mater. Syst. Struct.* **27** 1939–48
[31] Alexander R M 2005 Models and the scaling of energy costs for locomotion *J. Exp. Biol.* **208** 1645–52
[32] Wan X and Song S 2004 A cam-controlled, single actuator-driven leg mechanism for legged vehicles *Int. Mechanical Engineering Congress and Exposition* pp 1287–92
[33] Kim S and Wensing P M 2017 Design of dynamic legged robots *Found. Trends Robot.* **5** 117–90